

PAPER • OPEN ACCESS

Water-filled heat pipes for CubeSat thermal control

To cite this article: H J van Gerner *et al* 2021 *IOP Conf. Ser.: Mater. Sci. Eng.* **1139** 012003

View the [article online](#) for updates and enhancements.

You may also like

- [Water and xenon ECR ion thruster—comparison in global model and experiment](#)
Yuichi Nakagawa, Hiroyuki Koizumi, Yuki Naito *et al.*
- [Review of in-space plasma diagnostics for studying the Earth's ionosphere](#)
Luis Fernando Velásquez-García, Javier Izquierdo-Reyes and Hyeonseok Kim
- [Demonstrating High-precision Photometry with a CubeSat: ASTERIA Observations of 55 Cancri e](#)
Mary Knapp, Sara Seager, Brice-Olivier Demory *et al.*



UNITED THROUGH SCIENCE & TECHNOLOGY

 **The Electrochemical Society**
Advancing solid state & electrochemical science & technology

**248th
ECS Meeting**
Chicago, IL
October 12-16, 2025
Hilton Chicago

**Science +
Technology +
YOU!**

**SUBMIT
ABSTRACTS by
March 28, 2025**

SUBMIT NOW

Water-filled heat pipes for CubeSat thermal control

H J van Gerner^{1*}, H Brouwer², Z de Groot² and J Guo³

¹NLR – Royal Netherlands Aerospace Center, Voorsterweg 31 Marknesse, Netherlands

²ISIS – Innovative Solutions In Space, Motorenweg 23 Delft, Netherlands

³Faculty of Space Engineering, University of Technology Delft, Netherlands

Abstract. Currently, the amount of electrical power that is available for CubeSat's is very small and for this reason, simple thermal conductance through the frame of the CubeSat is sufficient for most CubeSat missions. However, deployable solar panels have been developed recently and peak powers up to 40W can now be generated. This higher generated electrical power results in more waste heat and potentially too high temperatures inside the CubeSat. For this reason, the use of water-filled heat pipes is studied, since these are cheap, widely commercially available, and can be bent in the desired shape. Both the condenser and evaporator thermal resistance and the total heat transfer capacity of these heat pipes have been measured for a wide range of temperatures with a unique automated setup that uses Peltier elements to control the temperature. Furthermore, the heat pipes have been subjected to multiple freeze/thaw cycles and start-ups from a frozen state. After these successful tests, a heat pipe was integrated in a CubeSat and tests were carried out in several orientations. The tests show that commercially available water-filled heat pipes are suitable for CubeSat thermal control.

1. Introduction

A CubeSat is small satellite which is made from a number of 10 cm x 10 cm x 10 cm units. Currently, the amount of electrical power that is available for CubeSat's is very small (~7W for a 3-unit CubeSat) and for this reason, simple thermal conductance through the frame of the CubeSat is sufficient for most CubeSat missions. However, deployable solar panels have been developed recently and peak powers up to 40W can now be generated [1]. This higher generated electrical power results in more waste heat and potentially too high temperatures inside the CubeSat. Ammonia-filled aluminum heat pipes are commonly used for larger satellites [2]. However, these are not suitable for CubeSat's because of their high costs. For this reason, the use of water-filled copper heat pipes is studied, since these are cheap, commercially available, and can easily be bent in the desired shape. Tests were carried out on axial-grooved and sintered heat pipes on the thermal resistance and heat transfer capacity of these heat pipes. These test results were used for the thermal model of a CubeSat with heat pipe [3]. The results discussed in this paper are for heat pipes with a length of 200 mm and an outer diameter of 6 mm. These heat pipes were bought from the German company Quick-Cool. Several heat pipes were cut in order to determine heat pipe characteristics and to study possible damage due to

* Corresponding author: Henk.Jan.van.Gerner@nlr.nl



freezing cycles. Figure 1 and Figure 2 shows cross-sections of two heat pipes. The work described in this paper has been carried out by Hugo Brouwer as part of his MSc. thesis [3].

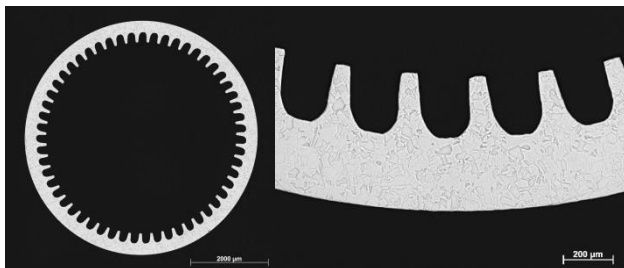


Figure 1. Cross-sections of an axial grooved heat pipe.

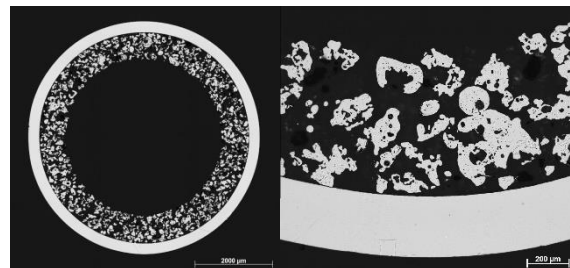


Figure 2. Cross-sections of a heat pipe with a sintered wick.

2. Test setup

Figure 3 shows the schematic drawing of the setup that is used to test the heat pipes, and Figure 4 shows a CAD drawing. The heater section consists of two copper blocks with cartridge heaters. The heat sink consists of two copper blocks between two Peltier elements which are cooled with a thermostat bath. Between the evaporator and condenser section is an adiabatic section with a length of 140 mm. The Peltier elements are used to maintain the saturation temperature of the heat pipe at the desired value, independent of the heat input (in contrast to more common setups, where the heat pipe temperature varies with the applied heater power). Two thermocouples are used to measure the evaporator section and condenser section temperature. These thermocouples have a diameter of 0.5 mm, and are inserted holes with a diameter of 0.6 mm. The adiabatic section has three thermocouples attached to the outside of the heat pipe. Under most conditions, the inside wall of the adiabatic section of the heat pipe is wetted with liquid water (with a strong thermal coupling to the vapor inside the heat pipe) and these three temperature sensors on the adiabatic section have approximately the same temperature, which is equal to the saturation temperature inside the heat pipe. When the inside of the heat pipe is not wetted with liquid water (e.g. due to a puncture, freezing, or dry-out), a large thermal gradient between the three temperature sensors can occur due to thermal conduction along the copper casing of the heat pipe. These three temperature sensors on the adiabatic section therefore give useful information about the functioning of a heat pipe.

The Peltier controller has its own dedicated temperature sensor in the middle of the heat pipe casing. The system is fully automated, such that a large dataset can be obtained with relative small effort. Figure 5 shows a photo of the setup with the insulation partly removed. In order to measure the heat leak from the setup, a test was carried out with a disabled heat pipe (with a hole drilled in the heat pipe casing). The following heat leaks were observed:

Table 1. Measured heat leak.

Heater power	Evaporator temperature
-	20°C (ambient temperature)
0.7 W	40°C
1.5 W	60°C
2.3 W	80°C

The heat leak scales linearly with the temperature difference between the heater block and the ambient temperature and is approximately 0.0375 W/K: This heat leak is negligible compared to the thermal conductance of a functioning heat pipe. The thermal conductance of the copper casing over

140 mm can be calculated to be 0.02 W/K. Most of the tests were carried out in horizontal orientation, although some measurements were carried out in a vertical or tilted orientation to investigate the influence of gravity.

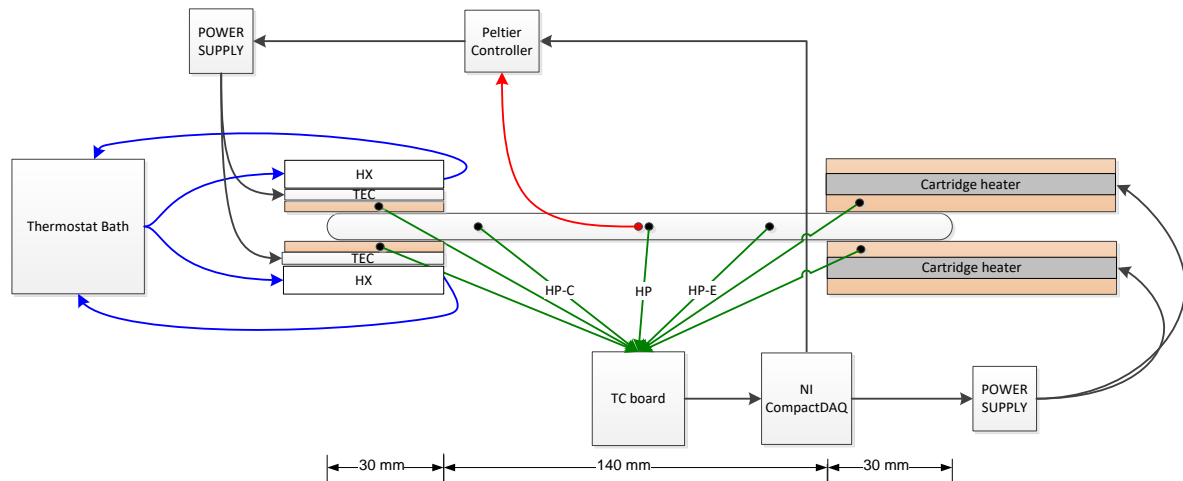


Figure 3. Schematic drawing of the test setup.

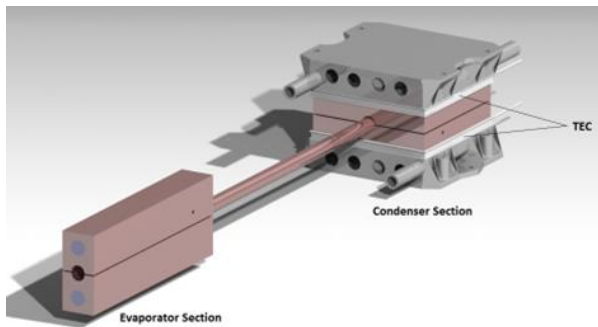


Figure 4. CAD drawing of the test setup.

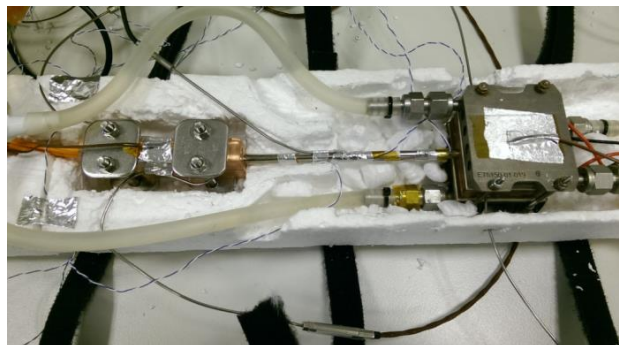


Figure 5. Photo of the test setup with insulation partly removed.

3. Capillary limit

There are several physical limits that restrict the heat transport capacity of heat pipes: the capillary limit, viscous limit, sonic limit, entrainment limit and the boiling limit [4, 5]. The capillary limit is often the most restrictive and can easily be calculated for axial grooved heat pipes. The maximum capillary pressure in an axial groove is

$$\Delta p_{\text{cap}} = \frac{2\sigma \cos \alpha}{d} \tag{1}$$

where σ is the surface tension of water, α is the contact angle between copper and water ($\sim 27^\circ$), and d is the width of the liquid channel (0.2 mm). The wicking height of the axial grooved heat pipe can then be calculated to be 66 mm. The effective pore diameter of the sintered heat pipe is approximately 0.1 mm, which results in a wicking height of approximately 26 cm. The frictional pressure drop due to laminar liquid flow in a square channel in an axial grooved HP is derived from the Hagen–Poiseuille equation:

$$\Delta p_{\text{friction}} = \frac{32 \mu L P}{\rho N d^4 H_{lv}} \tag{2}$$

where μ is the dynamic viscosity, L is the liquid transport length (approximately 170 mm), P is the heat input, ρ is the liquid density, N is the number of channels (55), d is the width and height of the channels (0.2 mm) and H_{lv} is the heat of evaporation. The fluid properties are obtained from [6]. By combining equation (1) and (2), the capillary limit of a heat pipe in horizontal orientation can be calculated. This calculated capillary limit is compared to the measured values in the next section. The capillary pressure scales linearly with d , while the frictional pressure scales with d^4 . This means that a smaller d results in a much smaller heat transport capacity (but a higher wicking height).

4. Thermal resistance measurements

4.1. Axial grooved heat pipe

The test setup was used to measure the heat transfer characteristics of the heat pipes. Figure 6 and figure 7 show the applied power and measured temperature during the test with the axial grooved heat pipe. The adiabatic section of the heat pipe has a nearly uniform temperature (the three temperature sensors on the heat pipe give nearly the same temperature, which is equal to the saturation temperature inside the heat pipe), which is held at a constant value by the Peltier elements, while the heat load is increased in small steps. This process is repeated for several heat pipe temperatures (e.g. 5 °C, 10 °C, 20 °C etc.). From these measured temperatures and heat input, the thermal resistance of several sections of the heat pipe can be derived. The thermal resistance of a heat pipe can be split in three parts:

1. Thermal resistance of the evaporator section i.e. between the temperature sensor in the heater (T_{evap}), and the adiabatic section ($T_{\text{HP-E}}$)
2. Thermal resistance of the adiabatic section, i.e. between the temperature sensor on the heat pipe near the heater section ($T_{\text{HP-E}}$) and near the condenser section ($T_{\text{HP-C}}$)
3. Thermal resistance of the condenser section i.e. between the adiabatic section ($T_{\text{HP-C}}$) and the condenser block (T_{cond})

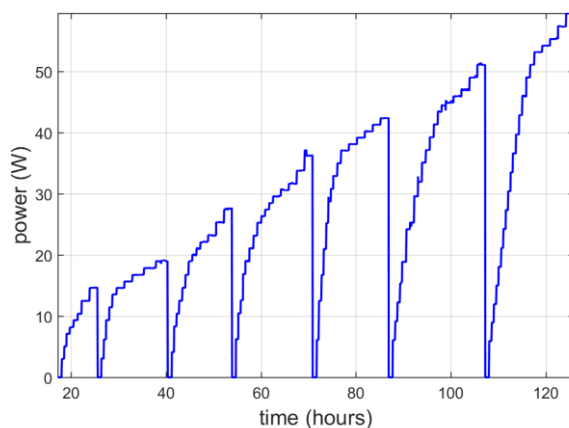


Figure 6. Applied heater power on the heat pipe.

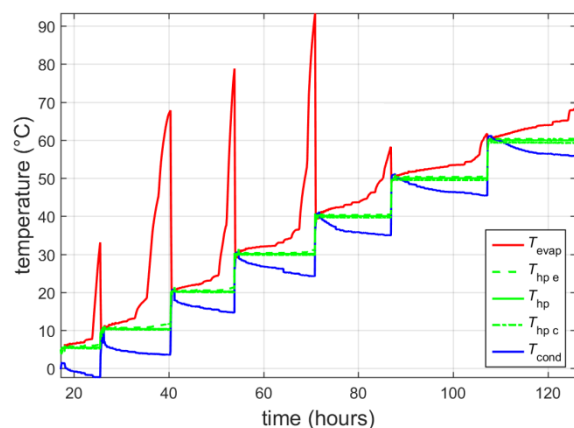


Figure 7. Measured temperatures on the copper heater block (red), three heat pipe locations (green), and the copper condenser block (blue).

The thermal resistance of the evaporator section is shown in Figure 8. The evaporator resistance decreases with temperature down to a value of 0.06 K/W. The resistance is relatively independent of heat input, until the capillary limit of the heat pipe is reached which results in a sharp increase in the resistance. For higher heat pipes temperatures (40° C, 50 °C and 60 °C) there is a good agreement between the calculated capillary limit and the measured sharp increase in thermal resistance. However, at lower heat pipe temperatures, the increase in thermal resistance occurs at a lower heat input than the calculated

capillary limit.

Figure 9 shows the thermal resistance of the adiabatic section. The thermal resistance is as low as 0.02 K/W. As a result of this low thermal resistance, the temperature difference over the adiabatic section is less than 0.5 °C for most measurements (see Figure 7). The thermal resistance of the copper heat pipe casing can be calculated to be 46 K/W, i.e. a functioning heat pipe ‘conducts’ heat more than 2000 times better than an empty heat pipe.

Figure 10 shows the thermal resistance of the condenser section. The condenser resistance is very high for low temperatures, so at low temperatures, the total resistance of a heat pipe is dominated by the condenser section. This can also be observed in Figure 7. This high resistance might be caused by the presence of a small amount of non-condensable gases inside the heat pipe which can block part of the condenser at low temperatures. Figure 11 shows the total thermal resistance of an axial grooved heat pipe.

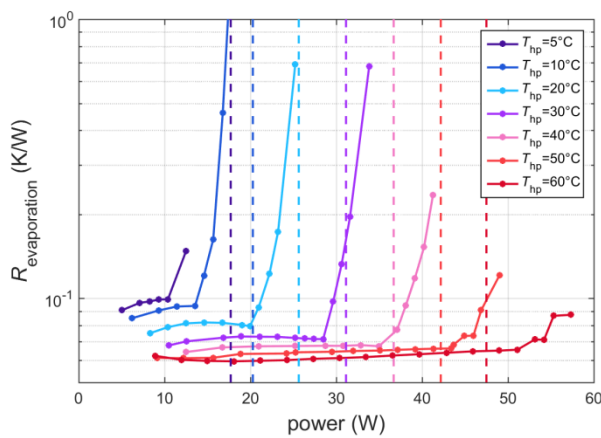


Figure 8. Condenser thermal resistance for an axial grooved heat pipe.

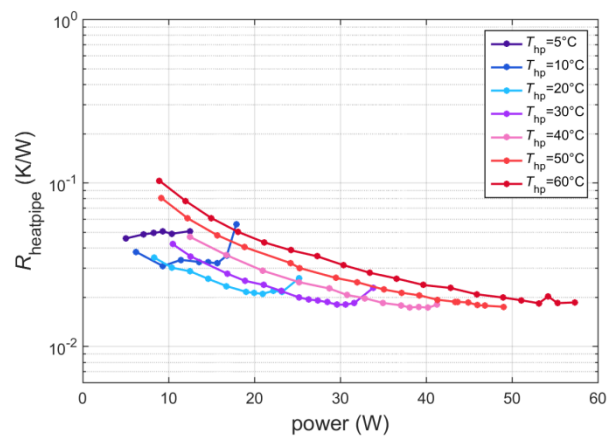


Figure 9. Total thermal resistance of an axial grooved heat pipe.

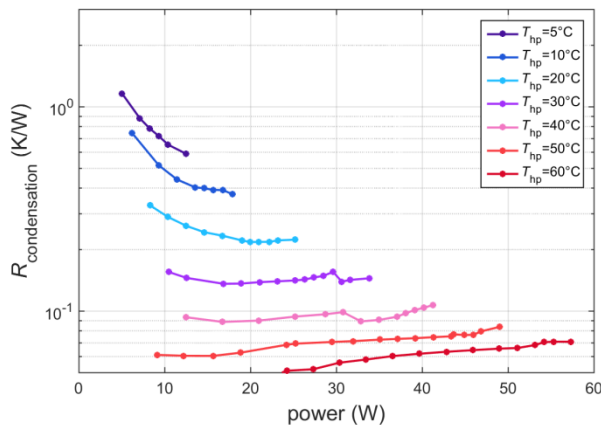


Figure 10. Condenser thermal resistance for an axial grooved heat pipe.

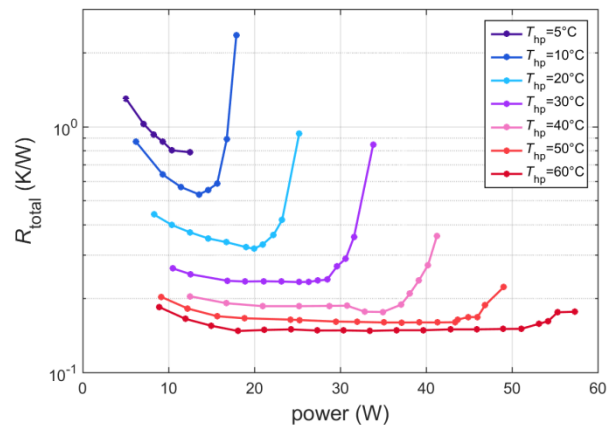


Figure 11. Total thermal resistance of an axial grooved heat pipe.

It is expected that the thermal resistance of the evaporator section and condenser section is inversely proportional to the interface area (since the thermal resistance does not strongly scales with heat flux). For heat pipe temperatures of 40°C or lower, the condenser thermal resistance is dominant over the other resistances, so the condenser interface area should be increased to lower the total resistance.

The decreasing evaporator and condenser thermal resistance at increasing temperatures results in the interesting phenomenon that the heater temperature can become lower when the heat sink temperature is increased (while maintaining the same heater power). For example, at a heater power of 36 W and a

heat sink temperature of 25 °C (heat pipe temperature is 30 °C), the evaporator block rises to over 90 °C. At the same heater power but with a heat sink temperature of 57 °C (heat pipe temperature is 60 °C), the evaporator block temperature is 62.6 °C. This means that when a heat pipe is applied, the heat source temperature can be decreased by increasing the heat sink temperature.

4.2. Sintered heat pipe

In the previous section, the heat transfer characteristics of an axial grooved heat pipe have been determined. Similar measurements have been carried out for sintered heat pipes with the same outer dimensions. Figure 12 shows the measured thermal resistance in the evaporator section, Figure 13 shows the thermal resistance of the adiabatic section, Figure 14 shows the thermal resistance in the condenser section and Figure 15 shows the total thermal resistance of the sintered heat pipe. For the sintered heat pipes, the capillary limit cannot be calculated since the permeability of the sintered material is not known. Compared to the axial grooved heat pipes, the sintered heat pipes have a much lower heat transport capacity because the frictional liquid pressure drop in the sintered wick is much larger than in the axial grooves. Also, the increase in thermal resistance when the capillary limit is reached is less sharp than for an axial grooved heat pipe.

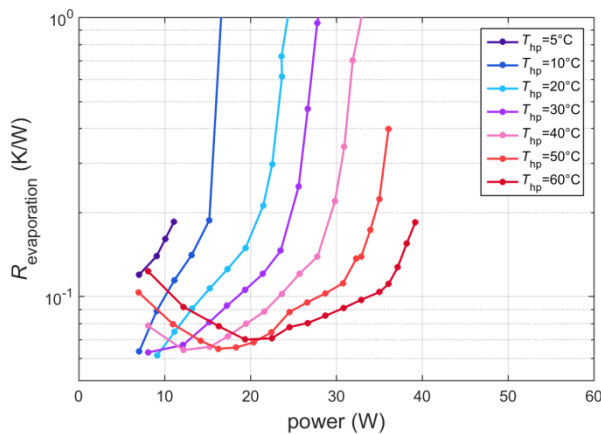


Figure 12. Evaporator thermal resistance for a sintered heat pipe.

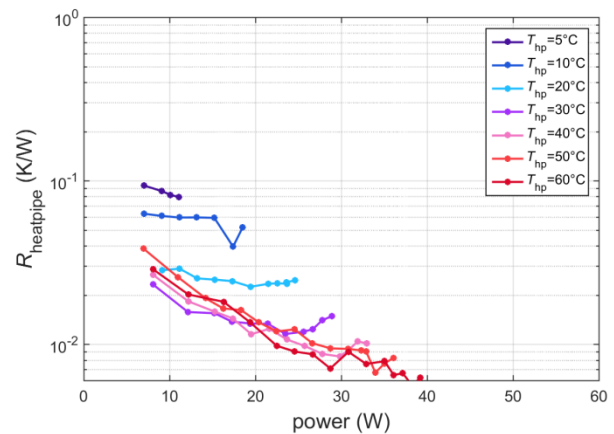


Figure 13. Thermal resistance of adiabatic section for a sintered heat pipe.

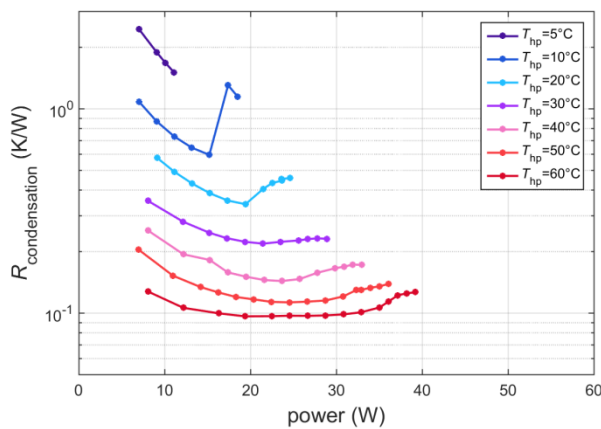


Figure 14. Condenser thermal resistance for a sintered heat pipe.

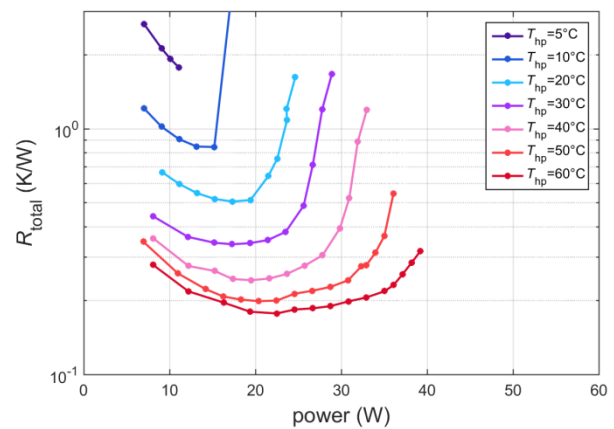


Figure 15. Total thermal resistance of a sintered heat pipe.

5. Freeze/thaw cycles

The radiator temperature of a CubeSat can become lower than 0°C , depending on orbit, radiator size and heat dissipation [3]. From literature, it is known that water-filled heat pipes can be damaged by multiple freeze-thaw cycles [7]. When the condenser section freezes, all the water in the heat pipe will accumulate in the condenser section, and when the condenser section thaws again, the heat pipe can be damaged by expansion of the liquid. Figure 11 in paper [7] shows a photo of a heat pipe that has ruptured at the condenser end of the heat pipe after 60 freeze/thaw cycles. This heat pipe has a length of 305 mm, an outer diameter of 4 mm and has a sintered wick. It was concluded that this damage was due to expansion of liquid from the frozen state. However, the heat pipes intended for CubeSats are shorter and have a larger diameter, and this makes it less likely that the heat pipe is damaged by freeze/thaw cycles.

Furthermore, an axial grooved heat pipe might be better suited to handle freeze/thaw cycles than a heat pipe with a sintered wick. For this reason, 100 freeze/thaw cycles were carried out for the axial grooved heat pipe (see Figure 16) and 82 for the sintered heat pipe (the test sequence for the sintered heat pipe was stopped before 100 cycles were reached because of a software crash). In each cycle, the condenser is set to -15°C for 15 minutes, and then to 10°C for another 10 minutes. Every 10 cycles, the condenser temperature is increased to 30°C and 20 W of heater power is applied for 15 minutes to check the functioning of the heat pipe. Figure 17 shows a short section of the test with 10 cycles and two functional tests. When the condenser section is set to -15°C , the heat pipe temperature quickly drops to just above 0°C , after which the heat pipe stops functioning and the heat pipe slowly cools further due to conduction through the copper casing. Note that the evaporator section never drops below 0°C because of the very small heat leak ($\sim 0.7\text{ W}$, see table 1) between the ambient and the heat pipe. This corresponds to the calculated heat transport by conduction through the copper casing. For an application in CubeSats, this is very interesting, since it implies that only a very small amount of electrical heater power ($\sim 1\text{ W}$) is required to maintain the payload above 0°C .

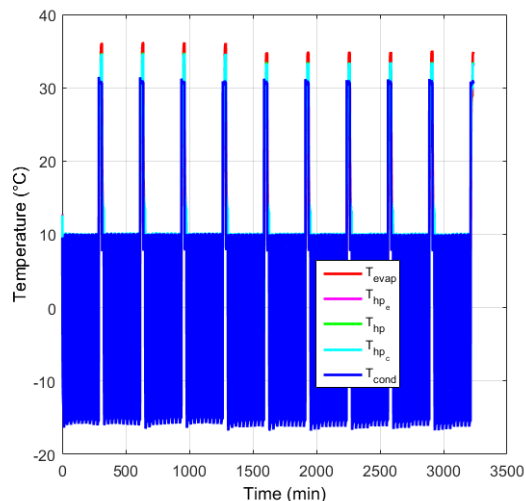


Figure 16 Measured temperatures during 100 freeze/thaw cycles. Every 10 cycles, the condenser temperature is increased to 30°C and 20W of heater power is applied for 15 minutes to check the functioning of the heat pipe.

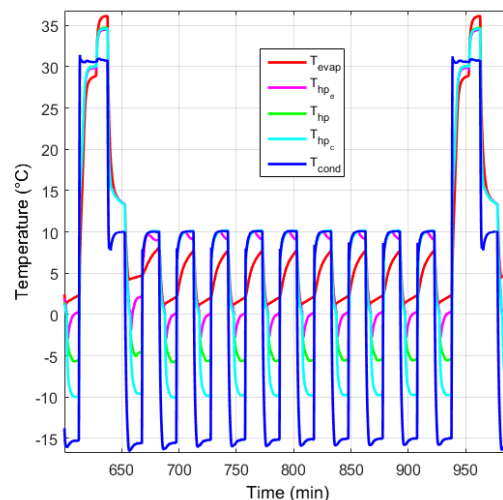


Figure 17. Zoom in on 10 cycles and 2 functional tests. See figure 3 for the location of the temperature sensors.

After the thermal cycling tests, both the axial grooved and sintered heat pipe functioned properly. Furthermore, cross section of the heat pipes (similar to Figure 1 and Figure 2) were made and the heat

pipes were internally inspected for damage. From these tests, it was concluded that the freeze/thaw cycles did not damage the heat pipes.

Start-up after freezing

Another issue is start-up of the heater from a frozen state. When the condenser section of the heat pipe is frozen, all water has accumulated in the condenser section and no liquid is present in the evaporator section. When a heat load is applied (by the payload), the heat will have to be transported by conduction through the copper housing until the condenser section is thawed and the heat pipe starts functioning again. However, since the thermal resistance of a non-functioning heat pipe is very high (~ 46 W/K), the payload might overheat before the heat pipe starts to function. Whether a heat pipe can be started from a frozen state without local overheating depends on the thermal inertia of the payload, the applied power, and the length and thermal conductance of the heat pipe casing [8]. Figure 18 shows the measured temperatures during a start-up test of an axial-grooved heat pipe with a frozen condenser section. After $t=6$ minutes, 10W of heat input is applied and the temperature of the evaporator section starts to rise. There is a temperature gradient over the adiabatic section of the heat pipe, which indicates that heat transport is mainly via conduction through the copper casing. Around $t=17$ minutes, part of the condenser starts to thaw, and the heat pipe starts to operate. At $t=26$ minutes, all the sensors on the adiabatic section have (nearly) the same temperature, which indicates that the heat pipe is functioning. This test shows that a start-up from a frozen state is possible without overheating of the heater section.

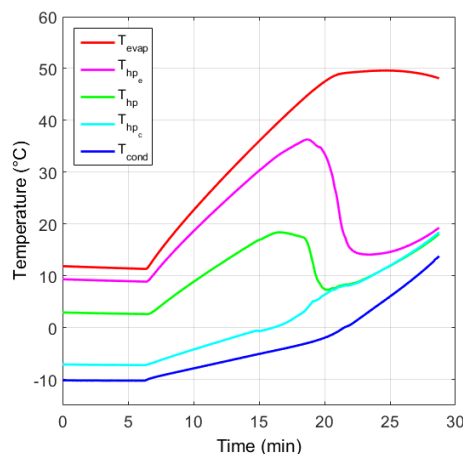


Figure 18. Measured temperatures during start-up from a frozen state.

6. Bending of heat pipes

For application of heat pipes in CubeSats, the heat pipes have to be bent. Two sintered, two axial-grooved, and two mesh heat pipes were bent (see Figure 19) with a bending tool with a bending radius of three times the heat pipe outer diameter. The heat transport capacity of these heat pipes was measured before and after the bending. No significant influence of the bending on the thermal performance of the axial grooved and sintered heat pipes was found. The heat transport capacity of the mesh heat pipe was greatly diminished after the bending. From these tests, it was concluded that the heat pipes can be bent with this bending radius.



Figure 19. Photo of 3 bended heat pipes.

7. Integration in CubeSat

After the successful thermal and bending tests, a heat pipe was integrated in a CubeSat (see Figure 20). The bending tool was not available during integration and the heat pipes were bended by hand. Tests were carried out in several orientations (both gravity-assisted and anti-gravity). Furthermore, start-up tests from a frozen condition were carried out. The tests (which are described in more detail in [9]) show that commercially available water-filled heat pipes are very suitable for CubeSat thermal control.



Figure 20. Photo of a CubeSat (with some panels removed) with a heat pipe.

8. Conclusions

The thermal resistance and heat transport capacity of heat pipes was measured and the correspondence with calculated values is reasonably well. The measured values have been used in a thermal model of a CubeSat to analyse its thermal behaviour [3]. No damage to the heat pipes was observed after 100 freeze/thaw cycles. The freezing of water in the heat pipe can even be an advantage, since it can protect the payload against too low temperatures. The tests show that commercially available water-filled heat pipes are suitable for CubeSat thermal control.

9. References

- [1] Weeren H, Brake M T, Hamann R, Holl G and Price S 2009 Thermal Aspects of Satellite Downscaling, *Journal of Thermophysics and Heat Transfer*, **23**, 592
- [2] Gilmore D G 2002 *Spacecraft Thermal Control Handbook. Vol I: Fundamental Technologies*, 2nd ed. ,The Aerospace Corporation, California
- [3] Brouwer H S B 2016 Performance Characterization of Water Heat Pipes and their Application in CubeSats, MSc. Thesis, <https://repository.tudelft.nl/>, Delft.
- [4] Peterson G P 1994 *An Introduction Into Heat Pipes: Modelling, Testing, and Applications*, John Wiley & Sons Inc.
- [5] Wits W W and Riele G J 2017 Modelling and performance of heat pipes with long evaporator sections. *Heat and Mass Transfer*, **53**(11):3341-3351
- [6] Lemmon E W, Huber M L, McLinden M O 2013 NIST Standard Reference Database 23: Reference Fluid Thermodynamic and Transport Properties-REFPROP, Version 9.1, National Institute of Standards and Technology, Standard Reference Data Program, Gaithersburg.
- [7] Cheung K 2005 Flight Qualification of Copper Water Heat Pipes At Naval Research Laboratory, *38th AIAA Thermophysics Conference*, Toronto (Ontario) Canada
- [8] Ochterbeck J and Peterson G 1994 Current Status of Frozen Heat Pipe Startup Research, *Proc. of the Tenth International Heat Transfer Conference*, Brighton, UK, 351–356.
- [9] Brouwer H, Groot Z D, Guo J, van Gerner H J 2017 Solving the Thermal Challenge in Power-Dense CubeSats with Water Heat Pipes, *Small Satellite Conference*, SSC17-VII-06